Proceedings of CONF-FMCE 2025 Symposium: AI and Machine Learning Applications in Infrastructure Engineering
DOI: 10.54254/2755-2721/2025.MH26395

Three-Dimensional Characterization and Quantitative Analysis of Sandstone Pore Structures Based on CT Scanning

Ruitong Dai

School of Geosciences, China University of Petroleum (Beijing), Beijing, China
2594598680@qq.com

Abstract. The pore structure of sandstone reservoirs is a key factor affecting hydrocarbon migration and accumulation. Accurately characterizing these features is of great significance for oil and gas exploration and development. This study selects two typical sandstones as research objects and employs CT scanning to obtain three-dimensional images. Through preprocessing, threshold segmentation, and quantitative algorithms, pore parameters are extracted. The correlation between two-dimensional porosity and three-dimensional porosity is analyzed, and the critical volume of the representative elementary volume (REV) is determined. Fractal dimension is also calculated to assess the complexity of the pore structure. This study aims to establish a method for three-dimensional quantitative characterization of sandstone pore structures, providing technical support for the precise analysis of complex reservoirs and offering guidance for oil and gas exploration and development.

Keywords: sandstone reservoir, pore structure, CT scanning, 3D characterization, fractal dimension, representative elementary volume (REV)

1. Introduction

Sandstone reservoirs are highly heterogeneous, possess complex pore structures, and generally have poor permeability. Since the pore structure of reservoirs is crucial for understanding hydrocarbon migration and accumulation, precise characterization of the pore system can strongly support oil and gas exploration and development.

Current conventional pore structure evaluation methods have limitations[1]. For example, mercury intrusion porosimetry may damage the rock sample[2]; gas adsorption methods cannot measure isolated pores[3]; and casting thin sections partially destroy the internal structure of the core and only reflect 2D pore-throat features. In contrast, the digital core analysis technology based on CT scanning allows for direct 3D imaging of sample pore structures without damaging the rock sample, thereby preserving its integrity. Prior research has confirmed the importance of CT scanning for 3D characterization of sandstone pore structures. Thanks to its voxel resolution and tomographic imaging capabilities, comprehensive and accurate internal pore structure information of sandstone can be obtained.

This study constructs a complete analytical framework based on CT scanning, covering image preprocessing to pore parameter quantification, to achieve precise 3D characterization of sandstone

© 2025 The Authors. This is an open access article distributed under the terms of the Creative Commons Attribution License 4.0 (https://creativecommons.org/licenses/by/4.0/).

DOI: 10.54254/2755-2721/2025.MH26395

pore structures. Specifically, geometric features of pores are extracted through threshold segmentation and algorithmic analysis. The relationship between 2D slice data and 3D imagery is explored, the minimum REV that reflects macroscopic physical properties is identified, and fractal dimension is applied to reveal the link between structural complexity and fluid flow capacity. Ultimately, the study provides reliable technical support and theoretical reference for research into hydrocarbon migration and practical reservoir development.

2. Data and methods

2.1. Data source

The images used in this study are sourced from the open-access rock sample database on the Digital Porous Media website. This database contains a large collection of CT-scanned rock data that have undergone standardized processing, covering samples with various lithologies, pore characteristics, and experimental conditions. All selected data have passed rigorous quality control procedures, including standardized scanning parameters (e.g., voxel resolution, scanning range) and image integrity verification, ensuring the comparability and reproducibility of data across different studies. The platform provides detailed sample preprocessing information, scanning equipment parameters (such as CT scanner model, X-ray energy, etc.), and the grayscale value range of the original images. This foundational information is critical for subsequent image preprocessing, threshold segmentation, and pore parameter extraction in this study.

Moreover, the open-source data from the Digital Porous Media website have undergone peer review and are widely recognized in the academic community for their scientific validity and reliability. They have been cited in numerous studies related to porous media characterization and fluid flow simulations, ensuring the authority and effectiveness of the data used in this research.

2.2. Sample information

Sample 1 is a mixed-wet Berea sandstone (Berea Altered: mixed-wet). The cylindrical sample has a diameter of 4 mm and a length of 20 mm[4]. First, the sample was saturated with brine (comprising 15% potassium iodide, 1.09% sodium chloride, 0.02% magnesium chloride hexahydrate, and 0.11% calcium chloride dihydrate by mass in deionized water). Then, oil displacement was carried out by injecting crude oil under a pressure gradient of 5 MPa. After injecting 2.5 mL of crude oil, the sample was immersed in crude oil and aged in an 80°C oven for 30 days. Subsequently, water flooding was performed at a flow rate of 0.015 mL/min and an injection pressure of 3.5 MPa, with a cumulative injection volume equivalent to 40 times the pore volume. In single-mineral systems, wettability is altered uniformly; however, in multi-mineral systems, minerals such as clay and calcite tend to become oil-wet, while quartz and feldspar remain relatively stable, resulting in mixed wettability[5]. Since Berea sandstone contains a variety of minerals (quartz, clay, calcite, etc.), it exhibits mixed wettability after the above treatment.

Sample 2 is a Bentheimer sandstone with altered wettability. The sample was processed into a cylindrical core with a diameter of 6.1 mm and a length of approximately 26 mm[6]. Two such samples were connected in series, forming a total length of 51.6 mm[7]. Initially, the samples were saturated with KI-containing brine, followed by centrifuge-assisted crude oil injection to achieve an initial brine saturation of about 10%[8]. The samples were then immersed in crude oil and aged for four weeks at 80°C under a pressure of 3 MPa to alter their wettability. After aging, the samples were mounted in a core holder, subjected to 2 MPa confining pressure, and displaced with decalin.

DOI: 10.54254/2755-2721/2025.MH26395

Oil and brine were injected sequentially at a total flow rate of 0.03 mL/min, with the brine fractional flow increasing from 0 to 1. After the pressure difference stabilized for at least 3 hours at each stage, a 10.7 mm downstream segment was scanned using a Zeiss Versa 510 X-ray microscope with a voxel size of 3.58 μm. The scanned images were then denoised and subjected to three-phase segmentation for further analysis.

2.3. Image preprocessing

To ensure the accuracy and stability of pore recognition, segmentation, and extraction, it is necessary to denoise the 2D grayscale images obtained from CT scanning. Noise artifacts caused by environmental factors typically appear as speckles, patches, or streaks. Common denoising methods include mean filtering, Gaussian filtering, median filtering, and bilateral filtering. However, the CT-scanned rock samples used in this study have already been denoised, and different phases have been marked using the watershed algorithm based on grayscale values. Therefore, additional preprocessing was not performed in this study.

2.4. Pore extraction and segmentation

In digital core analysis, threshold segmentation is employed to obtain binary pore images by setting different threshold values. There is often a clear difference in pixel grayscale between the target and background regions in the image. The threshold segmentation algorithm compares pixel grayscale values with a chosen threshold, assigning pixels above the threshold to the target (marked as 1) and those below to the background (marked as 0), resulting in a binary image containing only two pixel types. All pore extraction and subsequent processing in this study were conducted using Avizo 2019 software.

For Sample 1, the open-source data provides information on the material represented by each grayscale value (e.g., 2 = clay minerals; 3 = quartz-feldspar minerals; 4 = calcite cementation; 5 = other minerals; 6 = brine phase; 7 = oil phase). Thus, setting the intensity range to 6–7 allows the extraction of pore regions.

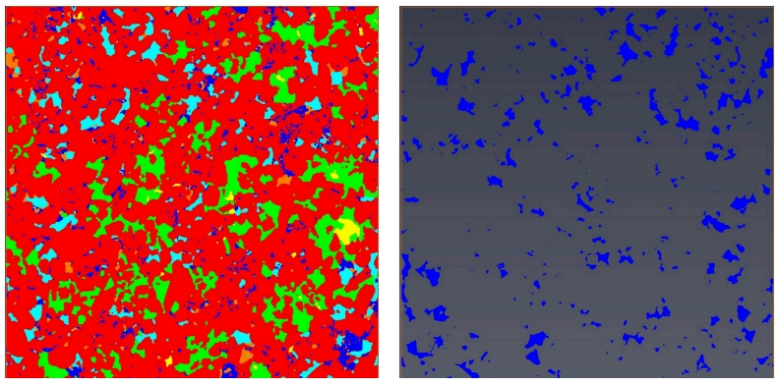


Figure 1. (a) Original image of Sample 1 with different colors representing different minerals or fluid phases; (b) Extracted pore regions (in blue) from image 1a

For Sample 2, the segmented 3D images indicate that rock grains are marked in red, brine phase in blue, and oil phase in yellow[9]. Setting the intensity range to 1–2 enables the extraction of pore regions.

DOI: 10.54254/2755-2721/2025.MH26395

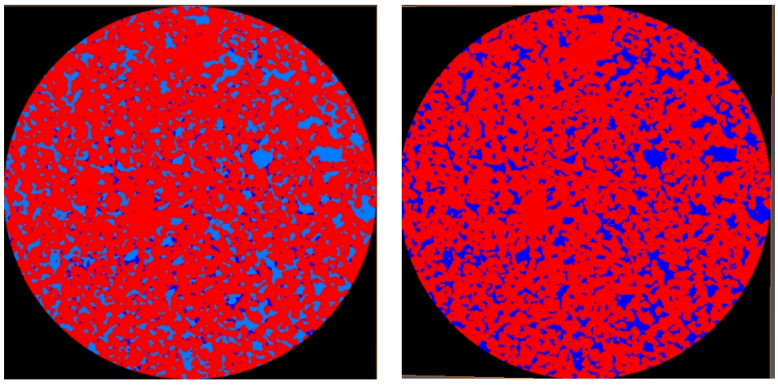


Figure 2. (a) Original image of Sample 2 with phase segmentation by color; (b) Extracted pore regions (in blue) from image 2a

2.5. Data processing methods

Based on the pore data extracted through threshold segmentation, Axis Connectivity algorithm in Avizo is used to identify connected pores. This algorithm assesses whether neighboring voxels within the target area (e.g., pores) belong to the same region along a specified axis (X, Y, or Z), thereby determining connectivity in that direction. This study focuses on extracting connected pores along the Z-axis. Next, the Label Analysis algorithm is applied to quantify the geometric features of the pores. Label analysis identifies regions with the same label after segmentation and calculates geometric (e.g., volume, surface area, diameter) and topological (e.g., connectivity) properties[10]. Here, the volume of each individual pore is of interest. Assuming each pore approximates a sphere, the equivalent radius is calculated based on geometric relations, thereby obtaining the pore size distribution in 3D. Finally, the Volume Fraction algorithm is used to compute both absolute porosity and connected porosity. This method involves identifying voxels that belong to the target region, counting their total number, and dividing by the total number of voxels in the analysis region to obtain the relative volume fraction—i.e., the porosity of the region

3. Three-dimensional pore structure characteristics

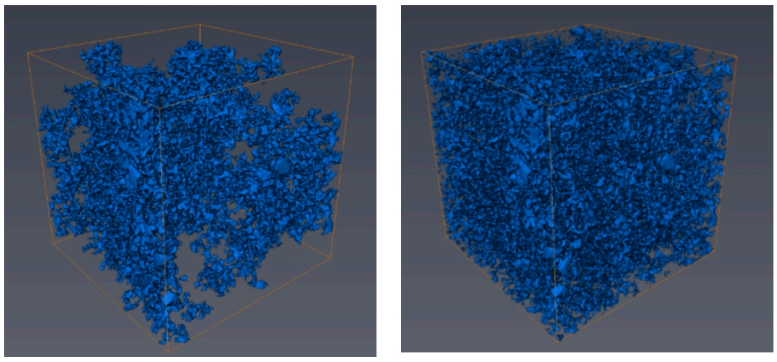


Figure 3. 3D pore structure of Sample 1: (a) All pores (left); (b) Connected pores (right)

DOI: 10.54254/2755-2721/2025.MH26395

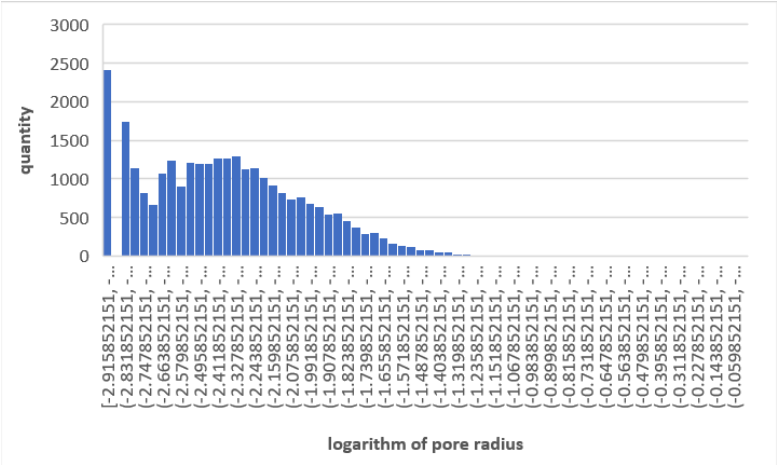


Figure 4. Histogram of pore radius (logarithmic) for Sample 1

The 3D pore structure of Sample 1 extracted from CT scans is shown in Figure 3. The total porosity is 7.35%, and the connected porosity is 4.63% (see Table 1). Due to the small pore radii, the logarithm of each radius is taken, and a histogram is plotted with a bin width of 0.08. As seen in Figure 4, the logarithmic pore radius distribution falls within the interval (−2.92, −1.23). In particular, the range (−2.7, −1.23) approximates a normal distribution, with a mean value around −2.33. A peak appears near −2.9, where approximately 2,400 pores are concentrated.

Table 1. Pore parameters for Sample 1

Average Pore Volume (mm³)	Average Radius (mm)	Absolute Porosity	Connected Porosity
3.29*10^(-5)	0.006418	7.35%	4.63%

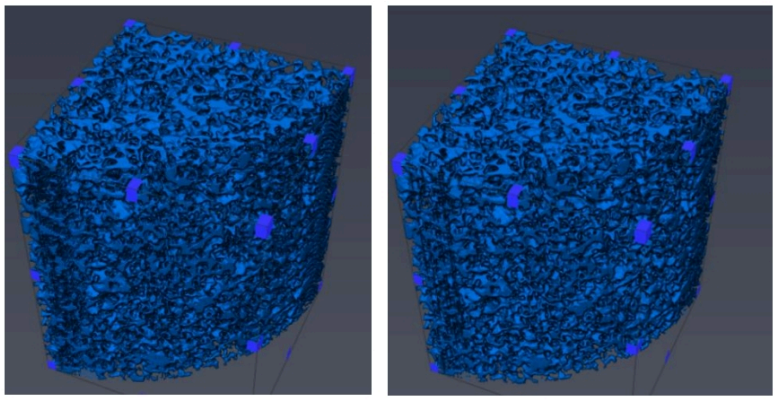


Figure 5. 3D pore structure of Sample 2: (a) All pores (left); (b) Connected pores (right)

DOI: 10.54254/2755-2721/2025.MH26395

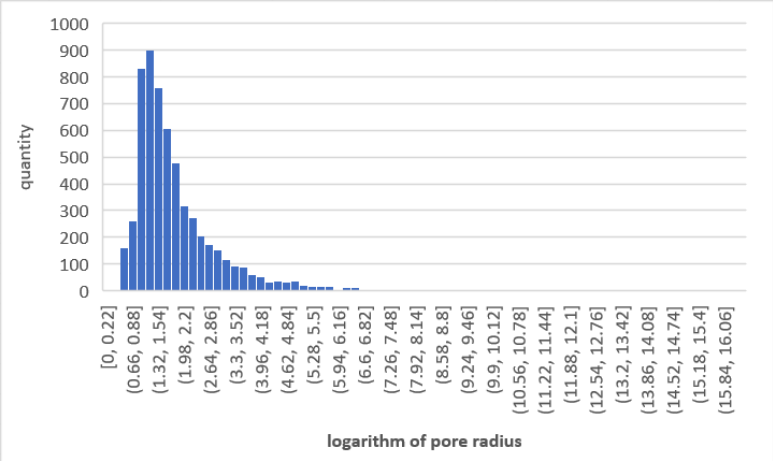


Figure 6. Histogram of pore radius for Sample 2

The 3D pore structure of Sample 2 is presented in Figure 5. The total porosity is 17.86%, and the connected porosity is 17.68% (see Table 2). Due to the large size of the pore data, the Extract Subvolume algorithm was used to select a sample with dimensions 1000 × 1000 × 1800 voxels, reducing computational cost. As shown in Figure 6, the number of pores peaks near a radius of 1.06 μm, reaching approximately 900 pores. The distribution curve is roughly normal with a small variance. Notably, connected pores account for 99% of all pores, indicating that almost no isolated pores are present.

Table 2. Pore parameters for Sample 2

Average Pore Volume (μm³)	Average Radius (μm)	Absolute Porosity	Connected Porosity
73.63	1.87	17.86%	17.68%

4. Discussion

4.1. Relationship between 2D structure and 3D image in pore characterization

2D pore structures often reflect the pore distribution on a specific slice of the rock sample. This subsection explores the relationship between the 2D porosity of different slices and the overall 3D porosity of the sample.

Using the formula: Porosity = number of pore voxels / total number of voxels, the porosity for each 2D slice in the XY plane along the Z-axis is calculated by setting the pore data obtained through threshold segmentation as the numerator and the raw sample data as the denominator. Then, by swapping the Y-axis with the Z-axis, the XZ-plane becomes the new XY-plane, and its 2D porosity is computed accordingly. Similarly, swapping the X-axis and Z-axis yields the 2D porosity of the YZ-plane[11].

DOI: 10.54254/2755-2721/2025.MH26395

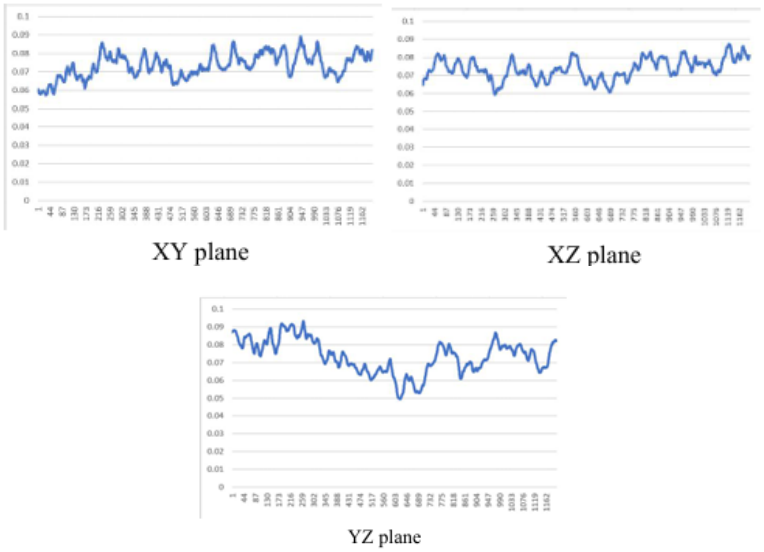


Figure 7. 2D porosity vs. slice index curves for the three planes

For Sample 1, Figure 7 shows the 2D porosity distribution curves along the X, Y, and Z directions. There are 1,200 slices in each direction. The surface porosity on the XY and XZ planes ranges from 6% to 9%, and that on the YZ plane ranges from 5% to 9%. The median values for the three directions are 7.37%, 7.29%, and 7.43%, respectively. Compared to the 3D porosity of the sample (7.35%), the difference is less than 1%.

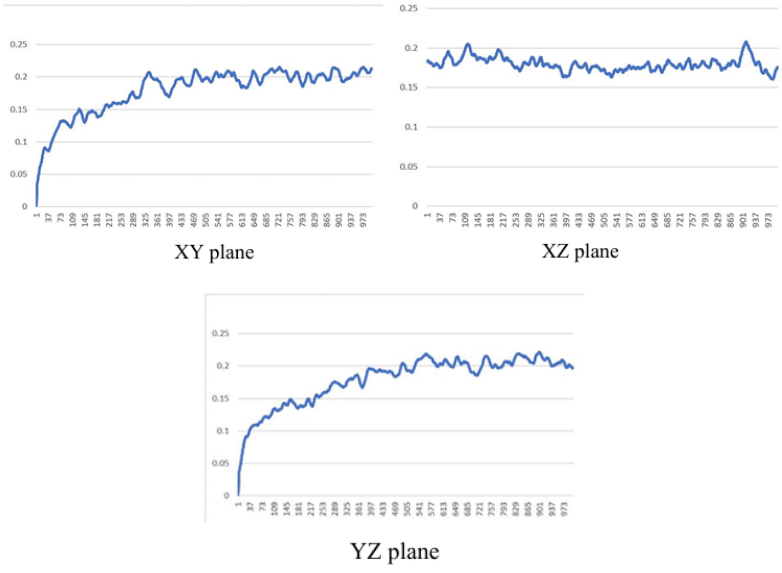


Figure 8. 2D porosity vs. slice index curves for Sample 2

Likewise, for Sample 2, the median values of surface porosity along the three directions are 17.83%, 19.45%, and 19.31%, respectively. These differ by less than 2% from the 3D porosity of 17.86%. Despite some fluctuations across different directions, the median value of 2D porosity can closely reflect the 3D porosity of the sample. This indicates that 2D image data can serve as an effective reference for 3D pore characteristics.

DOI: 10.54254/2755-2721/2025.MH26395

4.2. Representative Elementary Volume (REV)

A Representative Elementary Volume (REV) is the minimum volume of material that can represent its macroscopic physical properties (e.g., porosity, permeability, elastic modulus) without significant variation as volume increases. When the sample volume reaches or exceeds the REV threshold, local microscopic differences are statistically averaged out, and the measured physical properties become more accurate and stable. Thus, determining the REV volume prior to experimentation is crucial for the accuracy of measurements[12].

In this study, samples of decreasing volume were extracted from large to small using fixed intervals, and their porosity was calculated. The resulting data were plotted as a line chart. The point where the slope of the curve changes significantly indicates the REV threshold volume[13].

For Sample 1, the voxel size is 1200 × 1200 × 1200. Starting with the full volume, samples were sequentially reduced in steps of 50 × 50 × 50, and porosity was calculated at each step. As shown in Figure 9, the curve begins to fluctuate significantly after the 17th sampling scheme (with porosity of 6.85%), indicating that this is the REV threshold. The corresponding voxel size for this scheme is 400 × 400 × 400. Given that each voxel equals 8 μm³, the REV volume for Sample 1 is 0.512 mm³.

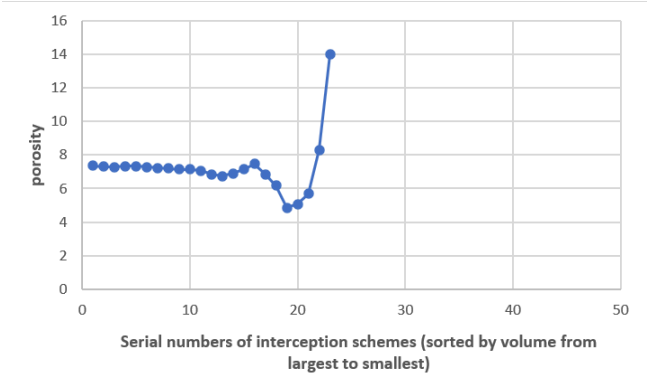


Figure 9. Porosity vs. extraction scheme curve for Sample 1

For Sample 2, the voxel size is 1600 × 1600 × 3000, and a subvolume of 1200 × 1200 × 2200 was used as the initial volume. The sampling interval was 50 × 50 × 100, and porosity was calculated for each subvolume. As shown in Figure 10, the curve drops sharply after the 5th sampling scheme, which is then identified as the REV threshold. This corresponds to a voxel size of 1000 × 1000 × 1800. Since each voxel equals 1 μm³, the REV volume for Sample 2 is 1.8 mm³.

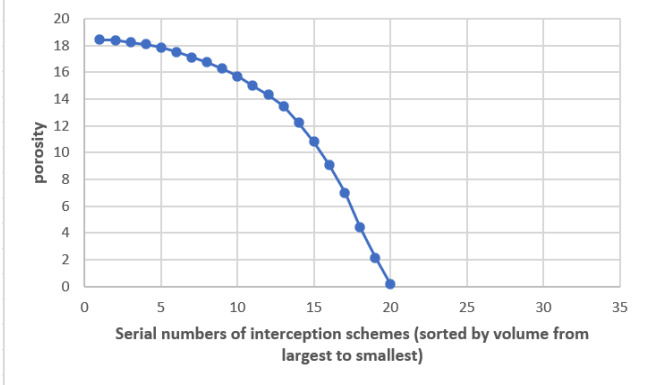


Figure 10. Porosity vs. extraction scheme curve for Sample 2

DOI: 10.54254/2755-2721/2025.MH26395

4.3. Fractal dimension

The fractal dimension is a quantitative measure of the complexity of irregular geometric forms[14]. It goes beyond traditional integer dimensions (e.g., 1D for lines, 2D for surfaces, 3D for solids) and is typically a fractional value. Its core concept is to evaluate the self-similarity of a structure across different scales, thereby reflecting its ability to fill space. The more complex the structure, the larger its fractal dimension. For 2D structures (e.g., pore contours), the fractal dimension ranges from 1 to 2; the closer it is to 2, the more densely the structure fills the plane. For 3D structures (e.g., pore networks in porous media), the fractal dimension ranges from 2 to 3; the closer it is to 3, the more intricate the structure is.

The box-counting method is commonly used to calculate the fractal dimension of 3D objects. This method involves filling the 3D object with cubes of varying edge lengths e, from large to small. The number of cubes required to fill the object is recorded as N(e), and the fractal dimension D is defined as: $D=\lim_{e\to 0}\frac{\log(N(e))}{\log(\frac{1}{e})}$.

For CT-scanned 3D rock sample data, consider a cubic sample with volume a × a × a. The cube used for filling (or “box”) has a volume of b × b × b. First, a binary image is obtained by applying threshold segmentation to the sample. Then, along the Z-axis, the sample is divided into (a/b + 1) slices at regular intervals. On each 2D slice, a grid of b × b cells is overlaid. The number of grid cells where the number of non-pore pixels exceeds half of the total in that cell is counted. Summing the counts from all slices yields the total number of boxes used to fill the structure, i.e., N(e)[15]. By varying the value of b, this process is repeated. A scatter plot of log(N(e)) versus log(1/e) is generated, and a linear regression is performed. The slope of the fitted line represents the fractal dimension of the sample. Using this method in Avizo software, the fractal dimension of Sample 1 was calculated to be 2.33, and that of Sample 2 was 2.56. This indicates that the pore connectivity pathways in Sample 2 are likely more tortuous than those in Sample 1.

There is no direct relationship between porosity and fractal dimension. Porosity reflects the storage capacity of the medium (e.g., oil-bearing capacity of rock), while fractal dimension relates to its transport performance (e.g., permeability, diffusion coefficient). For the same porosity, a higher fractal dimension indicates a more tortuous flow path, often leading to lower permeability. In petroleum geology, porosity is used to assess reservoir potential, and fractal dimension can further predict fluid flow efficiency. Together, they provide a comprehensive basis for reservoir evaluation.

5. Conclusion

(1) Compared with traditional pore structure evaluation methods, CT scanning technology offers significant advantages. It enables non-destructive imaging of sandstone samples, preserving the original morphology and internal structure of the pores, thus avoiding the damage often caused by conventional techniques. Through a series of image preprocessing and analytical algorithms, various pore parameters—such as pore volume, pore size distribution, and connectivity—can be accurately extracted, providing comprehensive insights into the pore structure of sandstone.

(2) The 2D porosity in different directions of a rock sample typically fluctuates within a certain range. However, by calculating the median 2D porosity along a specific direction, one can reasonably estimate the sample’s 3D porosity. This correlation suggests that 2D image data can effectively approximate 3D pore characteristics, offering a convenient approach for quickly assessing the macroscopic pore features of sandstone. Without the need for complex 3D image

DOI: 10.54254/2755-2721/2025.MH26395

analyses, one can obtain a preliminary understanding of pore conditions simply by processing 2D slice data—this holds significant practical value for initial reservoir assessments.

(3) When the sample volume reaches or exceeds a critical threshold, macroscopic physical properties—such as porosity—tend to stabilize. As such, accurately determining the REV volume is essential for reliable measurement of rock properties. Choosing a sample volume slightly larger than the REV allows for efficient use of material while still ensuring the accuracy of measurement results.

(4) A higher fractal dimension indicates a more complex pore structure and more tortuous pore connectivity paths. This characteristic is closely related to the fluid flow performance within the pores. A more intricate pore network increases flow resistance and affects the efficiency of hydrocarbon migration. Therefore, in reservoir evaluation, considering fractal characteristics can provide important insights into the dynamics of oil and gas movement.

References

[1] Xu, W., Liang, L., Gou, J., & Others. (2025). Characterization of pore structure of sand and conglomerate based on micro-CT scanning. Science Technology and Engineering, 25(3), 999–1007.
[2] Sun, X., Hu, G., Zhang, H., & Others. (2023). Characterization of pore structure and reservoir properties of tight sandstone with CTS, SEM, and HPMI: A case study of the tight oil reservoir in Fuyu oil layers of Sanzhao Sag, Songliao Basin, NE China. Journal of Petroleum Science and Engineering, 223, 111242.
[3] Li, X., Zhang, Z., Liu, Y., & Others. (2024). Evolution of pore structure and fractal characteristics in red sandstone under cyclic impact loading. Minerals, 14, 437.
[4] Garfi, G., John, C. M., Lin, Q., Berg, S., & Krevor, S. (2020). Fluid surface coverage showing the controls of rock mineralogy on the wetting state. Geophysical Research Letters.
[5] He, Z., Deng, L., Wang, H., & Others. (2024). Characteristics and influencing factors of pore structure in deep sandstone reservoirs: A case study of the Guai Lake Depression in the Yingen-Ejin Banner Basin. Journal of Peking University (Natural Science Edition), 60(2), 249–260.
[6] Li, J., & Xiao, L. (2024). A morphological method for predicting permeability in fractured tight sandstone reservoirs based on electrical imaging logging porosity spectrum. SPE Journal, SPE-219170-PA.
[7] Mao, W., Yao, Y., Qin, Z., & Others. (2024). Pore structure characterization of sandstone under different water invasion cycles using micro-CT. Geomechanics and Geophysics for Geo-Energy and Geo-Resources, 10, 53.
[8] Song, K., Wang, Y., Han, D., & Others. (2024). Study on the filling sequence of pores and fractures in tight sandstone reservoirs based on Wood's metal multi-level pressure injection experiments. Acta Petrolei Sinica, 45(9), 1239–1250.
[9] Lin, Q., Bijeljic, B., Berg, S., Pini, R., Blunt, M. J., & Krevor, S. (2019). Minimal surfaces in porous media: Pore-scale imaging of multiphase flow in an altered-wettability Bentheimer sandstone. Physical Review E, 99(6), 063105.
[10] Zhang, Y., Wang, Z., Li, H., & Others. (2023). Topological characteristics of the pore network in the tight sandstone using persistent homology. ACS Omega, 8, 46377–46385.
[11] Liu, S., Sun, W., Deng, B., & Others. (2020). Pore structure characteristics of the Xujiahe Formation sandstone reservoir in the Western Sichuan Depression and its influence on reservoir quality. Journal of Chengdu University of Technology (Science & Technology Edition), 47(2), 156–165.
[12] Wang, X., Du, Y., & Liang, X. (2021). Study on representative elementary volume of fractured rock mass based on heterogeneity coefficient. Hydrogeology & Engineering Geology, 48(2), 55–60.
[13] Li, X., Zhang, Y., Wang, F., & Others. (2024). Estimating and predicting the representative elementary volume of 3D fracture networks using an innovative computational framework and the dimensional harmony method. Engineering Geology, 319, 106936.
[14] Ma, Y., Zhao, J., Wang, C., & Others. (2023). Pore structure and fractal characteristics of tight sandstones based on nuclear magnetic resonance: A case study in the Triassic Yanchang Formation of the Ordos Basin, China. ACS Omega, 8, 10479–10489.
[15] Liu, K., Shi, W., Wang, R., & Others. (2021). Fractal characteristics of pore structure and its relationship with reservoir properties in the tight sandstone of He 1 Member in Hangjinqi area, Ordos Basin. Bulletin of Geological Science and Technology, 40(1), 57–68.